



# Historical trends and assessment of radionuclides and heavy metals in sediments near an abandoned mine, Lavrio, Greece

Filothei K. Pappa<sup>1,2</sup> · Christos Tsabaris<sup>1</sup> · Dionisis L. Patiris<sup>1</sup> · Effrosini G. Androulakaki<sup>1</sup> · Georgios Eleftheriou<sup>1</sup> · Chrysoula Betsou<sup>3</sup> · Veatriki Michalopoulou<sup>2</sup> · Michael Kokkoris<sup>2</sup> · Roza Vlastou<sup>2</sup>

Received: 11 May 2018 / Accepted: 15 August 2018 / Published online: 24 August 2018  
© Springer-Verlag GmbH Germany, part of Springer Nature 2018

## Abstract

Two sediment cores (coastal and offshore) and surface sediments were collected near an abandoned mine area in the marine environment of Oxygono Bay at Lavreotiki peninsula to investigate temporal and spatial variations among radionuclides and trace metals/major elements. Lavreotiki was and still is well known for the mining and metallurgical activities, which lasted from ancient times to nowadays (early 1980s). Gamma-ray and X-ray fluorescence measurements were held to determine the radionuclide and trace metal/major element concentrations, respectively. The sedimentation rate at Oxygono Bay coastal core was determined using the <sup>210</sup>Pb and <sup>137</sup>Cs tracers, while the enrichment factors were estimated to assess the anthropogenic influence due to metals in a spatial (surface sediments) and a temporal (coastal core sediments) basis. The mass flux at the coastal core was utilized to provide a baseline information at Lavreotiki peninsula. The trace metal/major element profiles were indeed associated with the mining activity in the area, revealing the mining history. The ERICA Tool was incorporated to estimate the dose rates due to natural and <sup>137</sup>Cs radioactivity in the marine organisms and the values were found below the screening levels.

**Keywords** Marine sediments · Heavy metal and radionuclide profile · Enrichment factors · Mass fluxes · Sedimentation rate · Lavrio

## Introduction

Metals are abundant in the environment due to either natural or anthropogenic processes, such as mining. Mining activities affect relatively small areas; they can have however a large local impact on the environment due to secondary sources of metals like tailings, waste rock deposits close to the mining

areas, smelter stacks, and atmospheric deposition (Salomons 1995; Li et al. 2006; Shukurov et al. 2014). During mining procedures, ore concentrating, mine tailing, wastewaters, and dust can be produced. The wastes are exposed to physical and chemical weathering processes (oxygen, water, and bacteria), so they can become heavy metal source for water in streams (Li et al. 2006), lakes (Becker et al. 2001; Kerfoot et al. 2004) and groundwater (Yellishetty et al. 2009), soils (Li et al. 2006; Batista et al. 2007; Yellishetty et al. 2009; Li et al. 2014), plants (Li et al. 2006; Batista et al. 2007), and sediments (Rowan et al. 1995; Batista et al. 2007; Villa et al. 2011; Kusin et al. 2017). Generally, at metallic mines, the heavy metal studies performed concern the aforementioned matrices. However, very few well-documented studies regarding the association of metal mines (e.g., Zn, Cu, Fe) with natural occurring radioactive materials (NORMs) exist, especially in the sediment near marine areas.

The NORM concentrations are investigated usually near coal (Balogun et al. 2003; Michalik 2008; Huang et al. 2015; Noli and Tsamos 2017), phosphate (Gaafar et al. 2016; Hassan et al. 2016), uranium (Salbu et al. 2013; Skipperud et al. 2013; Sethy et al. 2014), oil (Heaton and

---

Responsible editor: Georg Steinhauser

---

**Electronic supplementary material** The online version of this article (<https://doi.org/10.1007/s11356-018-2984-0>) contains supplementary material, which is available to authorized users.

---

✉ Filothei K. Pappa  
fkpappa@hcmr.gr

<sup>1</sup> Institute of Oceanography, Hellenic Centre of Marine Research, 46.7 km Athens-Sounio Ave, 19013 Anavyssos, Attiki, Greece

<sup>2</sup> Department of Physics, National Technical University of Athens, Zografou, 15780 Athens, Greece

<sup>3</sup> Department of Physics, Aristotle University of Thessaloniki, 54124 Thessaloniki, Greece

Lambley 1995; Hilal et al. 2014), and gold (Odumo et al. 2011; Ademola et al. 2014) mines. Usually, industrial activities generate as a by-product significant masses of NORMs, with similar or different chemical characteristics as the raw material and with higher concentrations of radioactivity due to the mass reduction within a process (Michalik 2008). In these waste masses, other pollutants like heavy metals might have been concentrated during the physical, mechanical, and chemical procedures of the ore product extraction. Nevertheless, as mentioned above, very little studies refer to NORM concentrations at metal mines (Pires do Rio et al. 2002; Saari et al. 2007; Arogunjo et al. 2009; Liu and Pan 2012) especially near/at marine environment (Villa et al. 2011; Pappa et al. 2016).

It should be noted that in near mine areas, the most studied matrices are soil and sediment. Both serve as a sink for metals and contain the depositional record of metal pollution. Thus, surface and core sediments can provide spatial and temporal information of the study area. Frequently, core sediments have been used for the metal accumulation and pollution assessment, the description of past environmental conditions, and the investigation of history contamination (Valette-Silver 1993) based on well-established radiological methods such as  $^{210}\text{Pb}$  (Sanchez-Cabeza and Ruiz-Fernandez 2012). The spatial and temporal investigation is important not only for ongoing but also for abandoned mines, as the impact due to mining activities may continue in the area due to the sorption characteristics of sediments and the remaining wastes. Thus, plant, biota, soil, and sediment (surface and core) studies have been incorporated in abandoned metallic mines worldwide to investigate the post-mining effect (Komnitsas et al. 1995; Rowan et al. 1995; Larsen et al. 2001; Navarro et al. 2008; Bech et al. 2012; Gomez-Gonzales et al. 2015; Garcia-Ordiales et al. 2017).

In the present study, a coastal area near an abandoned mining region at Lavreotiki Peninsula, eastern Attica, Greece, is investigated regarding the post-mining impact in the marine environment. The wider area of Lavrio bears mixed sulfide ore bodies developed along contacts of schist with marble (Kontopoulos et al. 1995). More specifically, the Pb-Ag-Zn massive sulfide mineralization of Lavrio is composed of Ag-bearing galena ( $\text{PbS}$ ), pyrite ( $\text{FeS}_2$ ), sphalerite ( $\text{ZnS}$ ), arsenopyrite ( $\text{FeAsS}$ ), and chalcopyrite ( $\text{CuFeS}_2$ ). Some of the secondary minerals are fluorite ( $\text{CaF}_2$ ), barite ( $\text{BaSO}_4$ ), carbonates ( $\text{CaCO}_3$ ,  $\text{CaMg}(\text{CO}_3)_2$ ), and quartz ( $\text{SiO}_2$ ) (Alexakis 2011). Even though the proposed method for reconstruction of past events was applied only for the past 200 years, a brief description of the history of the mine operation at Lavrio peninsula is introduced, as the impact of the pre-industrialized mining was still evident before the intense mining and metallurgical activities taking place in Lavrio. The area of Lavrio is one of the ancient mining districts with mining and processing activities for over 2700 years (Kontopoulos et al. 1995; Xenidis et al. 2003; Demetriades 2010). Extensive Ag-galena mining has

occurred since 3000 BC up to the 1980s (Alexakis 2011) involving the production of silver and lead from the exploitation of either carbonate or sulfide ores. Over 3500 t of Ag and  $14 \cdot 10^5$  t of Pb was produced in ancient times, 70% of which during the fifth and fourth centuries BC. The activities declined during the third century and stopped in the first century BC. The mining activities began in the middle of the nineteenth century and lasted until 1980s (Kontopoulos et al. 1995).

The intensive mining and metallurgical activities over the past 100 years for the production of lead and silver resulted in the production of huge volumes of wastes, which act as pollution sources and contribute to the widespread contamination of soils and water (Kontopoulos et al. 1995; Stamatis et al. 2001; Demetriades 2010; Alexakis 2011). The wastes such as slags, tailings, and low-grade ore were deposited in piles around Lavrio area, near the coastline or dumped into the sea (Stamatis et al. 2001; Alexakis 2011). The city of Lavrion is inhabited today by 10,000 people and was developed close to the waste stockpiles. The followed industrial and urban development led to the expansion of residential areas on the top of waste stockpiles. Thus, epidemiological studies conducted in the wider urban area of Lavrio revealed that, for 95% of children, Pb levels in blood exceed the tolerable limit of  $100 \text{ mg l}^{-1}$  suggested by the World Health (Xenidis et al. 2003). The wastes identified in the area were classified into three main categories: sulfidic flotation residues or tailings ( $8 \cdot 10^5 \text{ m}^3$ ), tailings from hydromechanical separation stages containing mainly oxidic-carbonaceous-silicates ( $5 \cdot 10^6 \text{ m}^3$ ) or pyritiferous tailings, and metallurgical slags ( $7 \cdot 10^6 \text{ t}$ ) (Kontopoulos et al. 1995; Demetriades 2010), exhibiting different geochemical and environmental characteristics (Xenidis et al. 1997; Xenidis et al. 2003; Demetriades 2010). More recent geochemical studies applied in Lavrio port revealed high concentrations in the outer pier area, due to the utilization of materials from earlier and ancient smelting disposal for the pier construction (Haralambides and Sakellariadou 2008). Additionally, one of the Lavrio bays, Thorikos, was remediated for the reduction of the Acid Mine Drainage (AMD) phenomenon occurring in the bay (Panagopoulos et al. 2009). Even though, Lavrion area has been studied for contamination reasons regarding mine wastes, soil, streams, groundwater, dust, animals, plants, urine, blood, and teeth of children (Stamatis et al. 2001; Aberg et al. 2001; Xenidis et al. 2003; Demetriades 2010; Alexakis 2011), there are little well-documented studies in the marine environment (Zotiadis and Keleperzis 1997; Sakellariadou and Haralambides 2004; Michalopoulou et al. 2015).

The present work was based on a preliminary investigation held in 2014 at the coastal areas of the eastern part of Lavreotiki Peninsula. During that study, four main bays near Lavrio port and Thorikos remediated site were examined for natural and metal concentrations, revealing the maximum concentrations at Oxygono Bay. Therefore, further investigation

in the marine area was incorporated at Oxygono beach, taking into account the spatial and temporal distribution in the bay. Thus, the main objectives of this work were: (a) the history reconstruction near the abandoned mine at the adjacent coastal area of Lavrio city, (b) the assessment of radionuclide and heavy metal concentrations using guideline values, the status of neighboring areas and enrichment factors, (c) to provide baseline information regarding the mass metal fluxes in the region, and (d) to estimate the dose rate assessment in non-human biota applying the ERICA Assessment Tool.

## Materials and methods

### Study area and field work

Two sampling surveys were held in the east part of Lavreotiki peninsula in 2014 and 2016. The preliminary survey was held in 2014, where surficial samples of beach sand and marine (coastal) sediments were selected at four bays Delenia, Oxygono, Thorikos, and Perdika, in order to determine the most affected area due to mining activities in the adjacent

region of a remediated site, Thorikos. Among the aforementioned bays, Oxygono was selected for further investigation as the maximum concentrations were observed in this region. Therefore, two sediment cores, one near the coast and the other in the offshore, were selected in 2014 for the history reconstruction of the study area. The length of each core was about 52 cm. The coastal core was located 50 m from the coast and was collected by a diver. The offshore core was located at a distance of approximately 1880 m from the coast and was collected by the HCMR's research vessel "Aegaeo," using a core sampler. The maximum depth of the offshore core was selected as the background level of the area, as it exhibited the minimum observed concentrations for the studied trace metals. Additional five surficial coastal sediments (approximately 2-cm depth) were collected at Oxygono Bay, so as to determine the spatial distribution. The sampling locations are shown in Fig. 1 and their coordinates and sampling dates are presented in Table 1.

### Sample preparation

The preparation of the sediment sample included the cleaning from stones, shells, algae, and sediment grains greater than

**Fig. 1** The sampling stations along Lavreotiki peninsula (preliminary survey 2014 (Michalopoulou et al. 2015), main surveys 2014 and 2016) (see Table 1)

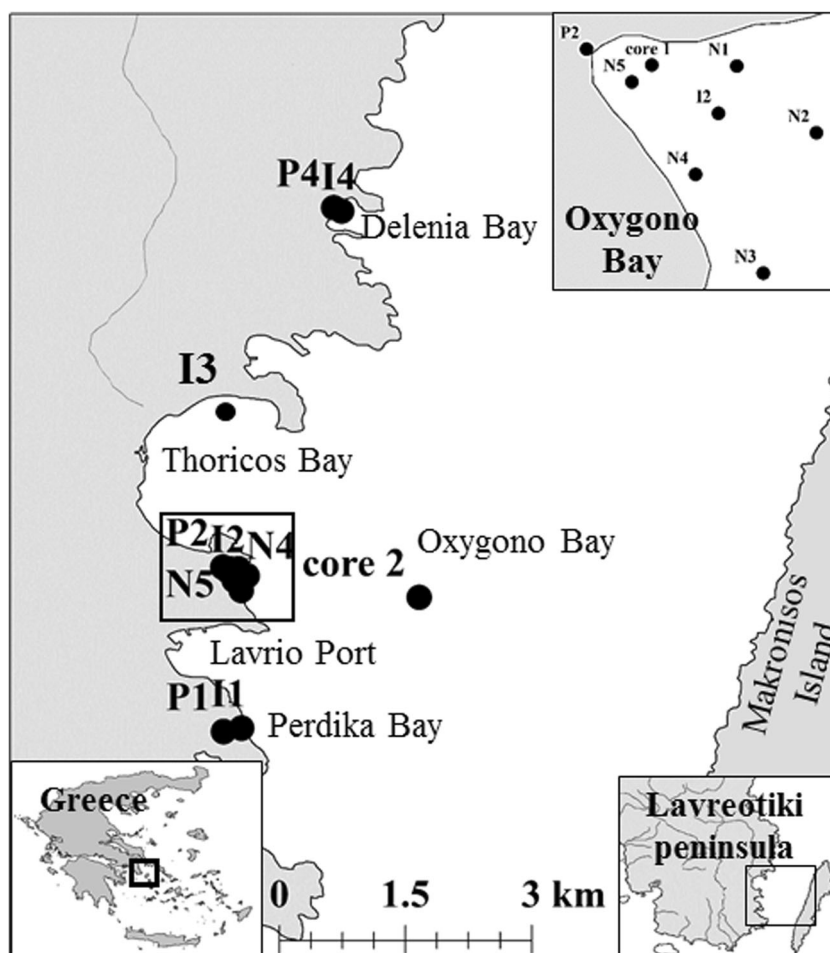


**Table 1** The sampling data

Sample	Latitude	Longitude	Sampling date	Depth (m)	Comment
Core 1	37° 43.173' N	24° 3.772' E	12 April 2014	4.5	52 cm length
Core 2	37° 42.990' N	24° 4.990' E	10 April 2014	45	52 cm length
N1	37° 43.173' N	24° 3.830' E	26 October 2016	Surface	Seafloor
N2	37° 43.128' N	24° 3.884' E	26 October 2016	Surface	Seafloor
N3	37° 43.033' N	24° 3.848' E	26 October 2016	Surface	Seafloor
N4	37° 43.100' N	24° 3.802' E	26 October 2016	Surface	Seafloor
N5	37° 43.162' N	24° 3.759' E	26 October 2016	Surface	Seafloor
I1	37° 42.145' N	24° 3.849' E	17 January 2014	Surface	Seafloor
P1	37° 42.122' N	24° 3.734' E	17 January 2014	Surface	Beach sand
I2	37° 43.141' N	24° 3.818' E	17 January 2014	Surface	Seafloor
P2	37° 43.185' N	24° 3.728' E	17 January 2014	Surface	Beach sand
I3	37° 44.269' N	24° 3.662' E	17 January 2014	Surface	Seafloor
I4	37° 45.479' N	24° 4.492' E	17 January 2014	Surface	Seafloor
P4	37° 45.502' N	24° 4.441' E	17 January 2014	Surface	Beach sand

2 mm. Thereinafter the drainage, sieving and pulverization of the remaining sample followed. From the powder, sample 80 g, 5 g, and 0.6 g were used for the radionuclide, major element, and trace metal measurements, respectively. The described procedure is presented in detail in Pappa et al. (2016).

## Radionuclide and metal analysis

### Analytical techniques

The gamma-ray measurements for the sediment cores (core 1 is the coastal and core 2 the offshore) were realized using a high-purity germanium detector (HPGe), at the Nuclear Laboratory of Physics Department of National Technical University of Athens (NTUA) (Canberra GC5021, 50% nominal relative efficiency). The determination of  $^{210}\text{Pb}$  activity concentration for the coastal core (core 1) was achieved by means of a Ge planar detector (GL 2020R) at the Department of Physics of the Aristotle University of Thessaloniki. The gamma-ray measurements for the surface sediments were performed with the broad energy HPGe detector (model ORTEC GEM-FX8530P4, 50% nominal relative efficiency) at Marine Environmental Radioactivity Laboratory (MERL) at the Hellenic Center for Marine Research. The powdered samples were placed inside cylindrical containers in touch geometry with the detector window (80 g and 7 g for cores 1 and 2 measurements, respectively). The offshore core (core 2) was mostly gravel (30–60%, see “Grain size analysis” section); therefore, the mass of the remaining sample (< 2 mm) appropriate for radioactive measurements was around 20 g. For this small quantity of mass and in order to be able to also measure metal concentrations, the small geometry (samples of 7 g) was used for the radioactive measurements. A lead shielding was surrounding the detectors so as to minimize the ambient gamma-ray background. The 24-h spectra were analyzed for

all the observed photopeaks of natural gamma-ray emitters and  $^{137}\text{Cs}$ . For the  $^{210}\text{Pb}$  measurements of core 1, spectra were acquired of 48 to 96 h, so as to reduce the statistical uncertainty.

All gamma-ray spectra were analyzed using the SPECTRW spectroscopy software package (Kalfas et al. 2016), and the analysis process (detector calibration, photopeak analysis, applied corrections) is described in Tsabaris et al. (2007), Pappa et al. (2016), and Patiris et al. (2016). In brief, the energy and photopeak efficiency calibrations were performed using as reference a voluminous source consisting of known activities of  $^{152}\text{Eu}$  (93%) +  $^{154}\text{Eu}$  (7%) prepared and calibrated at National Centre for Scientific Research (NCSR) “Demokritos.” The source was placed in touch geometry as the samples, so as to obtain spectra of gamma-rays in the range of 244 to 1408 keV. Additional reference sources  $^{235,238}\text{U}$  and  $^{40}\text{K}$  were used for the photopeak efficiency calibration in the low range energy from 63 to 100 keV and the higher energy of 1460 keV, which were produced using natural materials such as undisturbed soil of high natural radioactivity values and KCl whereby the stoichiometric ratio of  $^{40}\text{K}$  is known (Eleftheriou 2014). The absolute efficiency at the 46.5 keV, an important energy for  $^{210}\text{Pb}$  determination was estimated via a high-quality certified reference material RGU-1, with densities similar to the sediments measured after pulverization (IAEA 1987). The values were corrected for true coincidence summing effects using the EFFTRAN code (Vidmar et al. 2011). Special attention was paid to the analysis of the two-folded photopeaks at 186 keV, due to the contribution of  $^{235}\text{U}$  (185.7 keV) and  $^{226}\text{Ra}$  (186.2 keV) gamma-rays, respectively. The methodology of analysis is described elsewhere (Pappa et al. 2016; Patiris et al. 2016). Briefly,  $^{226}\text{Ra}$  activity was determined assuming secular equilibrium with its progenies ( $^{214}\text{Pb}$ ,  $^{214}\text{Bi}$ ). The  $^{226}\text{Ra}$  contribution was removed from the total counts of the two-



folded photopeak at 186 keV. The remaining counts were attributed to  $^{235}\text{U}$ . Additionally,  $^{235}\text{U}$  activity was also measured through 143.7 keV peak. This peak was clear from  $^{223}\text{Ra}$  (144.2 keV) contribution, as the samples were characterized by the absence of  $^{223}\text{Ra}$ . The main analyzed photopeaks utilized in this work can be found in Table S1 in the Supporting Information document. The uncertainty budget was determined taking into account the statistical uncertainty of the photopeak area, the gamma-ray intensities, the efficiency of the detection system, and the mass of the sediment sample.

The trace metal and major element concentrations were measured by a wavelength dispersive X-ray fluorescence (XRF) system WDXRF and the XRF spectra were analyzed using the Panalytical Pro-Trace software. The trace metal and major element concentrations of the samples were determined. The sample preparation, the samples' mass, the limit of determination, and the quality of the XRF method are described in Karageorgis et al. (2005).

### Dating analysis

The sedimentation rate (SR) estimation was incorporated on the collected sediment coastal core (core 1) through the vertical profiles of natural radionuclide  $^{210}\text{Pb}$  (Appleby and Oldfield 1978) and the artificial radionuclide  $^{137}\text{Cs}$  (Tsabaris et al. 2012). Briefly, the total activity concentration of  $^{210}\text{Pb}$  consists of a supported part due to  $^{226}\text{Ra}$  presence in the sediment of the sampling location and/or an unsupported (excess) part due to the transfer of  $^{222}\text{Rn}$  to the sampling location and subsequent sedimentation of aerosols containing also long-lived  $^{222}\text{Rn}$  daughter products. Thus, the unsupported (excess) portion ( $^{210}\text{Pb}_{\text{ex}}$ ) can be calculated by subtracting the activity concentration of  $^{226}\text{Ra}$  from the total activity of  $^{210}\text{Pb}$  so as to remove the supported portion. The constant flux-constant sedimentation (CF-CS) model was applied at the excess  $^{210}\text{Pb}$  profile for the SR estimation, as shown in Eq. 1:

$$\ln\left(\frac{A_0}{A}\right) = \frac{\lambda}{\text{SR}} z \quad (1)$$

where,  $A_0$  and  $A$  are the unsupported activity concentrations in the sediment core surface and the remaining depths of the sediment core ( $\text{Bq kg}^{-1}$ ), respectively,  $\lambda$  is the  $^{210}\text{Pb}$  radioactive decay constant ( $0.03114 \text{ y}^{-1}$ ),  $z$  is the depth (cm), and SR is the mean sedimentation rate of the selected core ( $\text{cm y}^{-1}$ ).

Regarding the  $^{137}\text{Cs}$  dating, the  $^{137}\text{Cs}$  peaks due to nuclear tests (1963) and Chernobyl accident (1986), observed in the  $^{137}\text{Cs}$  profile, allowed the estimation of the mean sedimentation rate according to Eq. 2:

$$\text{SR} = \frac{d_i}{(t-i)} \quad (2)$$

where,  $t$  is the year of the collected sediment core and  $d_i$  is the depth where the  $^{137}\text{Cs}$  peaks due to nuclear incidents ( $i = 1963, 1986$ ) were found.

The sedimentation rate estimation of the offshore sediment core (core 2) was not possible due to the difficulty of determining  $^{210}\text{Pb}$  and  $^{137}\text{Cs}$  activity concentrations. The gravel content of the samples, the small mass quantity of them (7 g), and the low activity concentrations of the aforementioned radionuclides, resulted in obtaining gamma-ray spectra of low statistics near the minimum detectable activity (MDA) of the detector's system and thus to the difficulty of  $^{210}\text{Pb}$  and  $^{137}\text{Cs}$  activity concentration determination.

### Grain size

The core sediment subsamples were split into sand and mud fractions by wet sieving through a  $63\text{-}\mu\text{m}$  mesh. The sand-mud separation was conducted, in order to investigate the grain size effect in the radionuclide and trace metal/major element concentrations.

### Enrichment factor

The enrichment factor (EF) is an approximation so as to estimate the anthropogenic influence above an uncontaminated background in the region of interest (Salomons and Forstner 1984). Therefore, the selection of uncontaminated background plays an important role as a reference. According to Birch (2017), among the empirical methods to establish the background value, the sample from a high-depth sedimentary core is proposed. Thus, the maximum depth (52 cm) of the offshore sediment core (core 2) was used as background value. The verification of this depth as a reference sample was confirmed by selecting a global—and not site specific—area for the EF determination. This global reference area was the shale of the earth's continental crust. The EF for the coastal core (core 1) and surface sediments was also calculated using as reference the shale of the earth's continental crust, so as to achieve site specific and global EF for the area of study. The most commonly used elements as normalizers are Al and Fe. In this work, Al was chosen. This element can be considered a non-anthropogenic element, which reduces the grain size effect in the sediment samples (Salomons and Forstner 1984). The EF definition is given by Eq. 3:

$$\text{EF} = \frac{\frac{M_{\text{sample}}}{\text{Al}_{\text{sample}}}}{\frac{M_{\text{ref.}}}{\text{Al}_{\text{ref.}}}} \quad (3)$$

where,  $M_{\text{sample}}$  and  $M_{\text{ref}}$  are the concentrations of the metal of interest in the sample and the reference sample, respectively, and  $\text{Al}_{\text{sample}}$  and  $\text{Al}_{\text{ref}}$  are the normalizer metal concentrations in the sample and the reference sample, respectively.

The classification adopted in this work is the one by Birch and Davies (2003) where seven classes are proposed:  $EF \leq 1$  indicating no enrichment,  $EF \leq 3$  a minor enrichment,  $3 < EF \leq 5$  a moderate enrichment,  $5 < EF \leq 10$  a moderately severe enrichment,  $10 < EF \leq 25$  a severe enrichment,  $25 < EF \leq 50$  a very severe enrichment, and  $EF > 50$  an extremely severe enrichment.

**Pollution load index**

According to Tomlinson et al. (1980), an empirical index was implemented, so as to characterize the level of metal pollution that is the pollution load index (PLI). PLI is calculated as

$$PLI = \sqrt[n]{CF_1 \times CF_2 \dots \times CF_n} \tag{4}$$

$$CF_i = \frac{M_{sample}}{M_{ref.}} \tag{5}$$

where, the contamination factor ( $CF_i$ ) of the  $i$  metal is the ratio of the metal concentration in the sample to the one of the reference sample and  $i = 1, 2, \dots, n$  is the number of metals of interest. This simplified index may assess the quality of the sediments as  $PLI \leq 1$  indicates no contamination or reveals the presence of contaminant baseline levels, while  $PLI > 1$  indicates progressive deterioration.

**Metal flux**

Usually, the geochemical and industrial input of metals into aquatic environment can be estimated by mass flux (MF) calculations in the sediment core incorporating the determined sedimentation rate. The excess mass flux estimation was applied for the coastal (core 1), since no sedimentation rate estimation was possible for the offshore sediment core (core 2). The MF calculation is given in Eq. 5 according to Cochran et al. (1998) and Spencer et al. (2003):

$$MF_i = (M_{xs})_i SR_i \rho_i \tag{6}$$

where,  $MF_i$  is the excess metal flux for the  $i$ th depth interval ( $\mu g y^{-1} cm^{-2}$ ),  $M_{xs}$  is the excess metal concentration for the  $i$ th depth interval ( $\mu g g^{-1}$ ),  $SR_i$  is the mean sedimentation rate at the  $i$ th depth interval ( $cm y^{-1}$ ), and  $\rho_i$  is the sediment dry bulk density ( $g cm^{-3}$ ).

In the present study, as baseline elemental concentration was considered the maximum depth of the offshore core (core 2). The excess metal flux ( $MF_i$ ) was determined by subtracting the elemental concentration of the  $i$ th depth from this baseline elemental concentration.

**ERICA assessment tool**

The dose rate calculation was performed for the marine organisms of Oxygono Bay using the ERICA Assessment Tool

(Brown et al. 2008). The natural and  $^{137}Cs$  activity concentrations in surface sediment were incorporated for the dose rate estimation, using the default parameters of the Tool, which are the dose conversion coefficient (DCC), the sediment-water distribution coefficient ( $K_d$ ), and the concentration ratio (CR). The  $^{40}K$  contribution was also taken into account in the dose rate assessment, as described in literature (Patiris et al. 2016; Pappa et al. 2016). In brief, the CR of Na element obtained from IAEA (2004) was used in place of the CR value of K and the sediment and seawater measurements at Oxygono Bay were also utilized for the  $K_d$  determination, as these parameters of K (CR,  $K_d$ ) are not included in the Tool. The  $^{40}K$  seawater measurement was achieved by the KATERINA underwater in situ detector system (Tsbaris et al. 2008). However, the activity concentration in the seawater of the other natural radionuclides ( $^{238}U$  and  $^{232}Th$  daughters) was below the MDA of the KATERINA system and thus, the default  $K_d$  values of these elements were used for the dose rate calculation. The estimated dose rates are not followed by an error. Nevertheless, in the present work, the confidence levels of the estimated values were determined. The upper and lower confidence levels were determined using the maximum and minimum activity concentrations of radionuclides, respectively according to the estimated relative uncertainty of the concentrations. In this work only, the uncertainty of the radionuclide activity concentration was taken into account for the uncertainty dose rate estimation.

**Results**

**Radionuclide and metal concentrations of surface sediments**

The activity concentrations of natural radionuclides ( $^{210}Pb$ ,  $^{226}Ra$ ,  $^{234}Th$ ,  $^{228}Ac$ ,  $^{235}U$ , and  $^{40}K$ ) and  $^{137}Cs$  at the surface sediments of Oxygono Bay are given in Table 2. The relative uncertainties of the aforementioned radionuclides were 10%, 7%, 9%, 13%, 7%, and 21%, respectively. The  $^{210}Pb$  activity concentration ranged from 42 to 112  $Bq kg^{-1}$  and the maximum value was observed at N5 station, the nearest sampling point to the coast. The activity concentrations of  $^{226}Ra$ ,  $^{228}Ac$ ,  $^{235}U$ ,  $^{40}K$ , and  $^{137}Cs$  did not exhibit any significant variation, providing mean values of 9, 13, 2.3, 159, and 1.3  $Bq kg^{-1}$ , respectively. The minimum values of  $^{226}Ra$  and  $^{228}Ac$  were observed in the south part of Oxygono Bay (N3, N4).  $^{234}Th$  was also determined and ranged among (30–47)  $Bq kg^{-1}$  characterized by uncertainties up to 16%. The surface sediments were collected and measured within a month. Thus the higher values of  $^{234}Th$  (around four times) compared to those of  $^{226}Ra$  may be attributed to the particle-reactive nature of thorium since sediment acts as a sink for thorium (Rose et al. 1994) or to the metal post-mining impact (Abril et al. 2018) and the secular equilibrium between  $^{234}Th$  and  $^{226}Ra$  cannot be assumed.

**Table 2** Activity concentration of  $^{210}\text{Pb}$ ,  $^{210}\text{Pb}_{\text{ex}}$ ,  $^{234}\text{Th}$ ,  $^{226}\text{Ra}$ ,  $^{228}\text{Ac}$ ,  $^{235}\text{U}$ ,  $^{40}\text{K}$ , and artificial radionuclide  $^{137}\text{Cs}$  in the surface sediments

Station	$^{210}\text{Pb}_{\text{tot}}$	$^{210}\text{Pb}_{\text{ex}}$	$^{234}\text{Th}$	$^{226}\text{Ra}$	$^{228}\text{Ac}$	$^{235}\text{U}$	$^{40}\text{K}$	$^{137}\text{Cs}$
Bq kg <sup>-1</sup>								
N1	42 ± 5	30 ± 5	30 ± 4	11.4 ± 0.6	14.0 ± 1.1	2.4 ± 0.3	184 ± 12	1.2 ± 0.2
N2	94 ± 8	84 ± 8	47 ± 6	9.5 ± 1.1	17.0 ± 1.2	1.3 ± 0.2	175 ± 11	1.2 ± 0.2
N3	50 ± 4	46 ± 4	32 ± 3	4.7 ± 0.3	10.2 ± 0.9	2.7 ± 0.2	136 ± 9	1.3 ± 0.4
N4	53 ± 6	47 ± 6	31 ± 3	6.6 ± 0.5	10.5 ± 1.5	3.0 ± 0.6	191 ± 12	1.2 ± 0.3
N5	112 ± 10	101 ± 10	29 ± 5	11.9 ± 0.5	13.2 ± 1.1	2.3 ± 0.3	111 ± 8	1.5 ± 0.4
World median <sup>a</sup>	–	–	–	35	30 <sup>b</sup>	–	400	–

<sup>a</sup> UNSCEAR (2000)<sup>b</sup> $^{232}\text{Th}$  decay series concentration

The concentrations of trace metals (As, Cu, Pb, Zn) and major elements (Mn, Al, Fe) are given in Table 3. The uncertainties of As, Cu, Pb, and Zn were 12%, 9%, 5%, and 5%, respectively and those of major elements were 5% for each element. The concentrations of As, Cu, Pb, and Zn ranged among  $(2.1\text{--}8.6) \cdot 10^3 \mu\text{g g}^{-1}$ ,  $(46\text{--}102) \mu\text{g g}^{-1}$ ,  $(2.3\text{--}3.9) \cdot 10^3 \mu\text{g g}^{-1}$ , and  $(4.9\text{--}12.5) \cdot 10^3 \mu\text{g g}^{-1}$ , respectively. The maximum concentrations for all trace metals were obtained at the nearest station to the coast, N5, while the minimum concentrations were measured at the south part of Oxygono Bay (N3, N4), like  $^{226}\text{Ra}$  and  $^{228}\text{Ac}$  activity concentrations. The spatial distribution of Mn and Fe exhibited also large variations, ranging from  $(4\text{ to }11) \cdot 10^3 \mu\text{g g}^{-1}$  and from  $(8\text{ to }21) \cdot 10^3 \mu\text{g g}^{-1}$ , where the maximum values were also observed at station N5. The Al concentrations in most sampling points were similar, exhibiting a mean value of  $19 \cdot 10^3 \mu\text{g g}^{-1}$ .

### Coastal core analysis (core 1)

#### Sedimentation rate

The sedimentation rate (SR) at the coastal core (core 1) was estimated using the  $^{137}\text{Cs}$  and  $^{210}\text{Pb}$  activity concentration profiles. The activity concentration of the excess  $^{210}\text{Pb}$  versus depth is depicted in Fig. 2. Due to the low concentration values of both radionuclides, the uncertainties for  $^{137}\text{Cs}$  and  $^{210}\text{Pb}$  activity concentrations were 21% and 24%,

respectively. Both methods revealed similar sedimentation rates of  $(0.26 \pm 0.01) \text{ cm y}^{-1}$  for  $^{137}\text{Cs}$  and  $(0.33 \pm 0.03) \text{ cm y}^{-1}$  for  $^{210}\text{Pb}$ . However, the latter sedimentation rate was used for the reconstruction of historical levels of metals and radionuclides at Oxygono Bay (see “[Historical reconstruction](#)” section), as the signals of Chernobyl accident and nuclear tests were not so distinct in  $^{137}\text{Cs}$  profile.

#### Grain size analysis

The sediment coastal and offshore cores were separated into slices of 2 cm. For each sample, analysis of the grain size distribution was performed. The results of the coastal core are shown in Fig. 3d and it was characterized as muddy sand according to Folk’s classification (Folk 1974). The whole core was mainly sandy and consisted of 80–100% sand and 0–20% mud. The only difference was observed in the middle part of the core, at 28–32 cm, where the sediment was finer and the mud portion reached 40%.

#### Radionuclide and metal concentrations of the coastal core (core 1)

The radionuclide and metal profiles of the coastal core (core 1) are depicted in Fig. 3a–c and Fig. S1a–S1h in the Supporting Information document. According to these profiles, the sediment core can be divided in three parts: the upper (0–28 cm),

**Table 3** Trace metal (As, Zn, Cu, Pb) and major element (Mn, Al, Fe) concentrations in the surface sediments

Station	As ( $\cdot 10^3$ )	Cu	Pb ( $\cdot 10^3$ )	Zn ( $\cdot 10^3$ )	Mn ( $\cdot 10^3$ )	Fe ( $\cdot 10^4$ )	Al ( $\cdot 10^3$ )
$(\mu\text{g g}^{-1})$							
N1	4.2 ± 0.5	70 ± 4	2.52 ± 0.12	7.2 ± 0.7	9.3 ± 0.5	12.7 ± 0.6	23.3 ± 1.2
N2	4.3 ± 0.5	74 ± 4	2.94 ± 0.14	7.4 ± 0.7	7.5 ± 0.4	12.4 ± 0.6	17.2 ± 0.9
N3	2.1 ± 0.3	46 ± 2	3.00 ± 0.14	5.7 ± 0.5	4.2 ± 0.2	7.8 ± 0.4	20.5 ± 1.0
N4	2.1 ± 0.3	50 ± 3	2.30 ± 0.11	4.9 ± 0.4	5.0 ± 0.2	8.0 ± 0.4	21.6 ± 1.1
N5	8.6 ± 1.1	102 ± 5	3.91 ± 0.18	12.5 ± 1.1	11.3 ± 0.6	20.6 ± 1.0	14.4 ± 0.7
Shale <sup>a</sup>	13	45	20	95	850	47 · 10 <sup>3</sup>	80 · 10 <sup>3</sup>

<sup>a</sup> Concentrations of shale of earth’s continental crust (Wedepohl 1995)

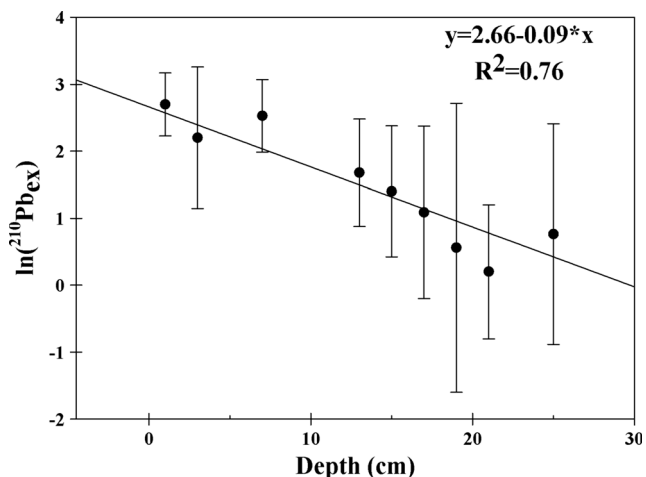


**Fig. 2** The sedimentation rate estimation at Oxygono Bay based on the unsupported  $^{210}\text{Pb}$  ( $^{210}\text{Pb}_{\text{ex}}$ )

the middle (28–38 cm), and the lower (38–52 cm). The activity concentrations of  $^{226}\text{Ra}$ ,  $^{235}\text{U}$ ,  $^{228}\text{Ac}$ , and  $^{40}\text{K}$  ranged between 4

and  $16 \text{ Bq kg}^{-1}$ ,  $8\text{--}16 \text{ Bq kg}^{-1}$ ,  $1.5\text{--}3.5 \text{ Bq kg}^{-1}$ , and  $130\text{--}200 \text{ Bq kg}^{-1}$  and their uncertainties were 9%, 16%, 21%, and 11%, respectively (Fig. 3a, Fig. S1a–S1c in the Supporting Information document). At the upper part, the values of  $^{226}\text{Ra}$  and  $^{228}\text{Ac}$  were found two times higher than those of the lower part, while in the middle part, they increased linearly between these values. However, homogeneous profiles, within uncertainties, were obtained for  $^{235}\text{U}$  and  $^{40}\text{K}$ , exhibiting mean values of  $2.5 \text{ Bq kg}^{-1}$  and  $180 \text{ Bq kg}^{-1}$ , respectively.

The As, Cu, Pb, and Zn concentrations ranged between  $(0.5\text{--}5.5) \cdot 10^3 \mu\text{g g}^{-1}$ ,  $40\text{--}220 \mu\text{g g}^{-1}$ ,  $(2.4\text{--}4.8) \cdot 10^3 \mu\text{g g}^{-1}$ , and  $(3.5\text{--}9.0) \cdot 10^3 \mu\text{g g}^{-1}$  and their uncertainties were 12%, 9%, 5%, and 5%, respectively (Fig. 3b, c, Fig. S1d and S1e of the Supporting Information document). As in  $^{226}\text{Ra}$  and  $^{228}\text{Ac}$  profiles, the As and Zn concentrations in the upper part of the core were six and two times higher than those in the lower part. However, in the Cu and Pb profiles, a peak was obtained in the middle part of the coastal core, at 28–

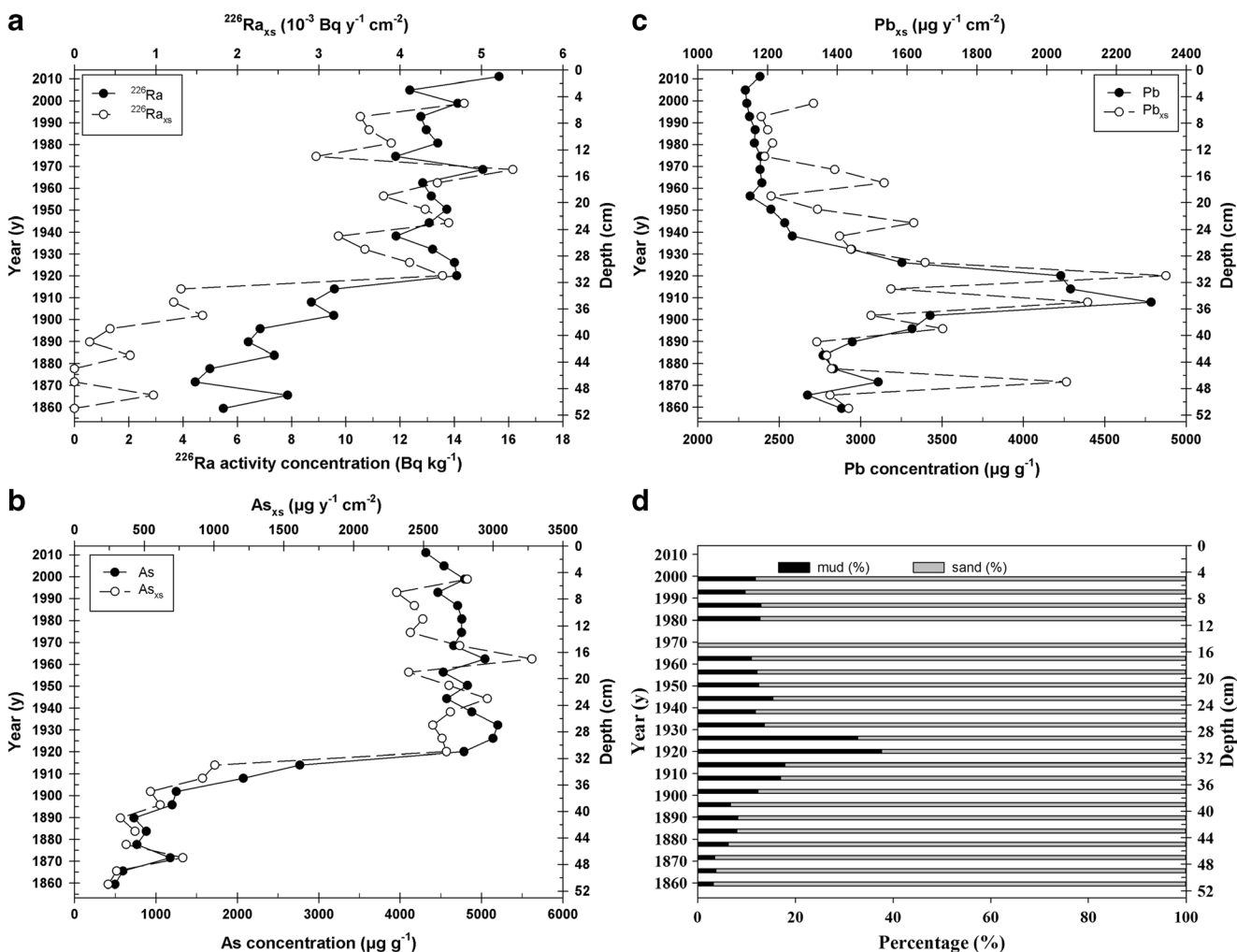


**Fig. 3** The concentrations of radionuclides ( $^{226}\text{Ra}$ ) and trace metals (As, Pb), along with their excess mass fluxes at the coastal sediment core (core 1). The mud-sand portion in the core, is also presented. **a** Activity

concentration and excess mass flux of  $^{226}\text{Ra}$ . **b** Concentration and excess mass flux of As. **c** Concentration and excess mass flux of Pb. **d** The mud-sand percentage



38 cm, where the concentrations were found three and two times higher than those in the upper and lower part of the core.

The Fe, Al, and Mn concentrations ranged between  $(2-15) \cdot 10^4 \mu\text{g g}^{-1}$ ,  $(1.4-2.3) \cdot 10^4 \mu\text{g g}^{-1}$ , and  $(1.5-11.0) \cdot 10^3 \mu\text{g g}^{-1}$ , respectively and their uncertainties were 5% for each element (Fig. S1f–S1h of the Supporting Information document). As in  $^{226}\text{Ra}$ ,  $^{228}\text{Ac}$ , and trace element profiles, the Fe and Mn concentrations in the upper part of the core were four times, for both elements, higher than those in the lower part. The values of As, Zn, Fe, and Mn in the middle part increased linearly between the concentrations of the lower part and those of the upper one. The values of Cu, Pb, and Al exhibited a peak with a maximum value during 1910–1930 (28–34 cm), which was 4, 2, and 1.5 times higher than those of the lower part, respectively. The Al concentrations varied in a lesser extent and were found at the upper part higher up to 20% than those at the lower part of the core.

### Excess metal flux

The trace metal and major element excess mass fluxes were determined in the coastal core, taking into account the sedimentation rate value, as obtained by incorporating the  $^{210}\text{Pb}$  and  $^{137}\text{Cs}$  dating methods. The excess metal flux profiles are depicted in Fig. 3b, c, as well as in Fig. S1d–S1h of the Supporting Information document, together with the trace metal/major element profiles. The excess mass fluxes of As, Cu, Pb, Zn, Fe, Al, and Mn ranged between  $(0.3-2) \cdot 10^3 \mu\text{g y}^{-1} \text{cm}^{-2}$ ,  $10-90 \mu\text{g y}^{-1} \text{cm}^{-2}$ ,  $(0.9-1.8) \cdot 10^3 \mu\text{g y}^{-1} \text{cm}^{-2}$ ,  $(1.3-4.5) \cdot 10^3 \mu\text{g y}^{-1} \text{cm}^{-2}$ ,  $(1.0-6.5) \cdot 10^4 \mu\text{g y}^{-1} \text{cm}^{-2}$ ,  $(3.0-4.5) \cdot 10^3 \mu\text{g y}^{-1} \text{cm}^{-2}$ , and  $(0.5-5.5) \cdot 10^3 \mu\text{g y}^{-1} \text{cm}^{-2}$ , respectively. For all metal distributions, the mass flux profiles exhibited similar trend as the concentration profiles.

The excess mass flux was also calculated for the long-lived natural radionuclides and their results are depicted in Fig. 3a and Fig. S1a–S1c of the Supporting Information document. Although  $^{228}\text{Ac}$  is not a long-lived radionuclide, the mass flux estimation can be considered as  $^{232}\text{Th}$  mass flux estimation, assuming secular equilibrium between them. The mass fluxes of  $^{226}\text{Ra}_{\text{xs}}$ ,  $^{228}\text{Ac}_{\text{xs}}$ ,  $^{235}\text{U}_{\text{xs}}$ , and  $^{40}\text{K}_{\text{xs}}$  ranged between  $(0-5.5) \cdot 10^{-3} \text{Bq y}^{-1} \text{cm}^{-2}$ ,  $(0-3) \cdot 10^{-3} \text{Bq y}^{-1} \text{cm}^{-2}$ ,  $(0-0.7) \cdot 10^{-3} \text{Bq y}^{-1} \text{cm}^{-2}$ , and  $(50-85) \cdot 10^{-3} \text{Bq y}^{-1} \text{cm}^{-2}$ , respectively. Similarly as in metal mass flux profiles, the radionuclide mass flux profiles exhibited the same trend as the concentration profiles.

### Offshore core analysis (core 2)

#### Grain size analysis

The offshore core is characterized as muddy sandy gravel according to Folk (1974). The gravel, sand, and mud portions ranged among 30–60%, 30–50%, and 10–20%, respectively.

### Radionuclide and metal concentrations of the offshore core (core 2)

The gamma-ray analysis of the offshore core was measured with large uncertainties due to the gravel content of the samples, the small quantity of sample mass, and the low values of activity concentrations. The low statistics spectra were analyzed; however, radionuclide profiles were very difficult to be obtained due to the discrepancies of the radioactivity concentrations and thus, only the activity ranges are presented in Table 4. The activity concentrations of  $^{226}\text{Ra}$ ,  $^{235}\text{U}$ ,  $^{228}\text{Ac}$ , and  $^{40}\text{K}$  found among the MDA of detector's system and up to  $18 \text{Bq kg}^{-1}$ ,  $6.7 \text{Bq kg}^{-1}$ ,  $18 \text{Bq kg}^{-1}$ , and  $300 \text{Bq kg}^{-1}$ , respectively with uncertainties 18%, 5%, 30%, and 6%, respectively. The low uncertainty of  $^{235}\text{U}$  at the offshore core (core 2) compared with the one of the coastal core (core 1) corresponds to the indirect calculation of its activity concentration via the 186-keV peak as described in Patiris et al. (2016). Thus, the  $^{235}\text{U}$  uncertainty derived from the square root of the remaining counts of the 186-keV peak, after the subtraction of  $^{226}\text{Ra}$  contribution. However, in the coastal core (core 1), the  $^{235}\text{U}$  activity concentration was determined using not only 186-keV peak but also other characteristic photopeaks of  $^{235}\text{U}$ . The activity concentration of  $^{137}\text{Cs}$  was below the MDA of the detection system.

Trace and Mn measurements were performed in the offshore core and they are depicted in Fig. 7. The As, Cu, Pb, Zn, and Mn ranged between  $20-80 \mu\text{g g}^{-1}$ ,  $8-20 \mu\text{g g}^{-1}$ ,  $40-200 \mu\text{g g}^{-1}$ ,  $40-200 \mu\text{g g}^{-1}$ , and  $150-500 \mu\text{g g}^{-1}$ , respectively. According to these measurements, the core can be divided in an upper (0–18 cm) and a lower (18–52 cm) part, where the values in the first part were found up to three times higher than those in the second part. The metal values in the offshore core were up to two orders of magnitude lower than those in the coastal core, as shown in Fig. 5, verifying a less influenced area due to past anthropogenic activities.

## Discussion

### Surface sediments

#### Comparison with neighboring areas and international values of reference

The minimum and maximum values of radionuclides obtained in surface sediments at Oxygono Bay, in 2014 and 2016 surveys, are given in Table 4 together with the world median values for soil (USEPA 2000). The radionuclide concentrations in the present study exhibited maximum values at Oxygono Bay and were similar to neighboring areas such as Perdica Bay, Thorikos Bay, and Delenia Bay. These values were found well below the world median for soil.

**Table 4** Comparison with neighboring areas, world median for radionuclides, the shale of continental crust of earth, and sediment quality guidelines. The uncertainty budget of natural radionuclides was 7%, 9%, 13%, and 7% for <sup>226</sup>Ra, <sup>228</sup>Ac, <sup>235</sup>U, and <sup>40</sup>K, respectively. The uncertainty budget of As, Cu, Pb, Zn, and Mn was 12%, 9%, 5%, 5%, and 5%, respectively

		Natural radioactivity				Heavy metals				
		<sup>226</sup> Ra (Bq kg <sup>-1</sup> )	<sup>228</sup> Ac	<sup>235</sup> U	<sup>40</sup> K	As (μg g <sup>-1</sup> )	Cu	Pb	Zn	Mn
Core 1 <sup>a</sup> (coastal core)	Min	4	8	1.5	130	500	40	2400	3500	1500
	Max	16	16	3.5	200	520,000	220	4800	9000	11,000
Core 2 <sup>a</sup> (offshore core)	Min	MDA	MDA	MDA	MDA	20	8	40	40	150
	Max	18	18	6.7	300	80	20	200	200	500
Oxygono B. (surf) <sup>b</sup>	Min	5	10	1.3	111	2100	46	2300	4900	4200
	Max	12	17	3.0	191	8600	102	3910	12,500	11,300
Oxygono B. <sup>a</sup>	Seafloor	10	8	<2.5	180	3400	120	3300	6900	7200
	Beach	20	7	<2.5	100	890	140	6000	8100	4300
Perdica B. <sup>a</sup>	Seafloor	<2	4	<2.5	70	50	8	200	100	340
	Beach	<2	<5	<2.5	80	70	15	390	180	950
Thorikos B. <sup>a</sup>	Seafloor	8	12	<2.5	230	—*	—	—	—	—
Delenia B. <sup>a</sup>	Seafloor	9	—	<2.5	340	35	13	120	144	330
	Beach	6	9	<2.5	300	34	12	150	150	390
Lavreotiki peninsula <sup>c</sup>	Min	—	—	—	—	6	3	20	15	—
	Max	—	—	—	—	2857	270	448	5763	—
world median <sup>d</sup>		35	30	—	400	—	—	—	—	—
av. shale <sup>e</sup>		—	—	—	—	13	45	20	95	850
OMEE <sup>f</sup>	SEL	—	—	—	—	33	110	250	820	1100
NOAA <sup>f</sup>	ERM	—	—	—	—	70	270	218	410	—
FDEP <sup>f</sup>	PEL	—	—	—	—	64	170	160	300	—
ISQG <sup>f</sup>	High	—	—	—	—	70	270	220	410	—
USEPA <sup>f</sup>	High	—	—	—	—	33	149	128	459	—
OMEE <sup>f</sup>	Lowest	—	—	—	—	6	16	31	120	460
NOAA <sup>f</sup>	ERL	—	—	—	—	8	34	47	15	—
FEDP <sup>f</sup>	TEL	—	—	—	—	8	28	21	68	—
ISQG <sup>f</sup>	Low	—	—	—	—	20	80	50	200	—

<sup>a</sup> Sampling in 2014

<sup>b</sup> Sampling in 2016

<sup>c</sup> (Zotiadis and Kelepertzis 1997)

<sup>d</sup> World median of soil (UNSCEAR 2000)

<sup>e</sup> Average continental crust (shale) concentrations (Wedepohl 1995)

<sup>f</sup> Sediment guidelines (SEL, severe effect level; ERM, effects range-medium; PEL, probable effect level; ERL, effects range-low; TEL, threshold effect level) (OMEE 1993), (USEPA 2000), (ANZECC 2000)

MDA, minimum detectable activity, \*The (—) means not available data

Additionally, the maximum metal concentrations of surface sediments in 2016 sampling were similar with the values of the coastal core and the surface sediments of Oxygono Bay in the 2014 sampling. Regarding the metal concentrations of the present study, they were well above those of the offshore core, the neighboring bays (Perdica, Delenia, Thorikos), the south east part of Lavreotiki peninsula (Zotiadis and Kelepertzis 1997), the shale of the continental crust (Wedepohl 1995), and the upper level of sediment quality guidelines (OMEE 1993; ANZECC 2000; USEPA 2000), indicating a bay

influenced by the mining and metallurgical activities occurred in the area. According to the literature (Panagopoulos et al. 2009), the neighboring bay of Thorikos was greatly influenced due to mining activities and therefore, it was remediated, which clarifies the low metal concentrations obtained at Thorikos Bay.

**Spatial distribution**

The interpolated spatial distribution of <sup>226</sup>Ra and PLI was estimated in Oxygono Bay incorporating the empirical

Bayesian Kriging (Gribov and Krivoruchko 2012) method via ArcGIS 10.2 software®. The utilized data were the ones of the surface sediments (2014 and 2016 sampling) and the surface sample of the coastal core (core 1). The limited number of data—seven points—provided only an indicative picture of the spatial distribution, as shown in Fig. 4. According to the spatial distribution, at Oxygono Bay, three distinctive regions can be observed (a) near N5 and core 1 surface samples, (b) at the north part of the bay, and (c) at the south part of the bay. The area most influenced from the mining activities was assessed to be near Oxygono beach, at N5 and core 1 surface samples and can be possibly associated with the elevated concentrations of radionuclides and metals in the beach sand sample (P2). Additionally, elevated concentrations of the aforementioned elements were estimated in the northern part of Oxygono Bay, while the minimum values were determined at the southern part of the bay, representing a less affected area. According to the literature (Kontopoulos et al. 1995), the southern terrestrial part of the bay was covered with metallurgical slags. However, a review study by Demetriades (2010), regarding the terrestrial—northern and southern—part of Oxygono Bay and the terrestrial area near sampling point P2 to be characterized with contaminated overburden and pyritiferous tailings, respectively. Moreover, the overburden and pyritiferous tailings were enriched in Pb, As, and other metals (e.g., Cu, Zn), as indicated by the spatial distribution of Pb and As and the contamination index in the same study. According to Demetriades (2010), the terrestrial more contaminated area at Oxygono Bay was mainly in the southern part. Thus, the elevated values of metals observed in the sediment, near the beach sand, and at the south Oxygono Bay via the interpolated spatial distribution may be associated with the waste distribution in the terrestrial part or with the water transfer contaminants originated from the neighboring gulf of Thorikos (see Fig. 1). The spreading out of the distribution

only in the southern—and not in the whole—bay may be related to the wind direction in the area of study. The spatial distribution of PLI values was similar to that of  $^{226}\text{Ra}$ , revealing a possible association among metals and radionuclides. The calculated PLI at Oxygono Bay indicated a progressive deterioration in the area according to Tomlinson et al. (1980), as all the PLI values were well above one.

### Enrichment factors

The enrichment factors (EFs) of heavy metals (As, Cu, Pb, Zn, and Mn) were estimated for the surface sediments of Oxygono Bay and are presented in Table 5. The EFs were determined using the elemental concentrations of the last depth of the offshore core (see “Enrichment factors” section for the assessment of core 2 last depth sample as reference). According to Birch and Davies (2003), the study area can be considered extremely severely enriched in As and Zn, very severely to extremely severely enriched in Pb, severely to extremely severely enriched in Mn, and minor to severely enriched in Cu. The order of enrichment was  $\text{As} > \text{Zn} > \text{Pb} > \text{Mn} > \text{Cu}$ . The sampling point with the maximum EF was the one near beach sand, N5, while the sampling point with the minimum enrichment was that at the southern part of Oxygono Bay, N3 and N4, verifying the spatial and interpolated spatial distribution of radionuclides and trace metals described in “Radionuclide and metal concentrations of surface sediments” and “Spatial distribution” sections, respectively.

### Dose rate assessment

The maximum activity concentrations measured at Oxygono Bay surface sediment were utilized for the dose rate calculation and potential radiological hazard assessment for the marine biota. The radionuclide concentrations of  $^{210}\text{Pb}$ ,  $^{226}\text{Ra}$ ,  $^{228}\text{Th}$ ,  $^{228}\text{Ra}$ ,  $^{235}\text{U}$ ,  $^{40}\text{K}$ , and  $^{137}\text{Cs}$  were inserted in the

**Fig. 4** **a** The spatial distribution of  $^{226}\text{Ra}$ . **b** The spatial distribution of pollution load index (PLI) calculated from the trace metal (As, Cu, Pb, Zn) and Mn concentrations.  $\text{PLI} \leq 1$  indicates no contamination or that the baseline levels of contaminants are present;  $\text{PLI} > 1$  indicates progressive deterioration (Tomlinson et al. 1980)

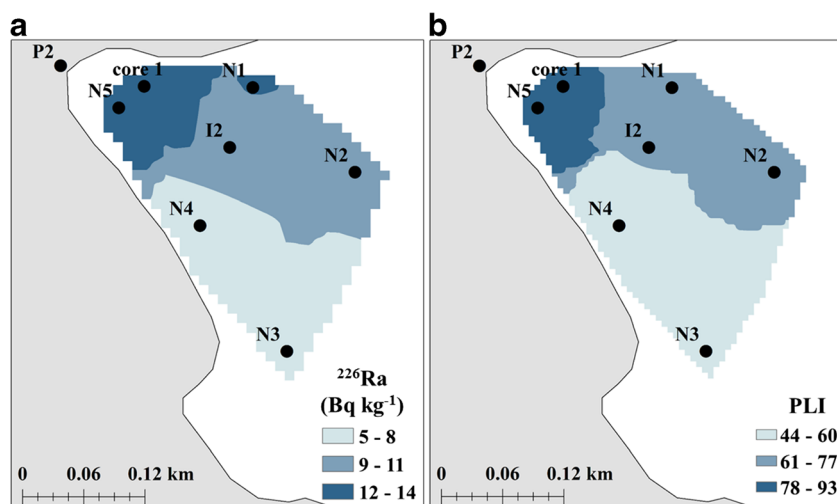


**Table 5** Enrichment factors (EFs) of surface sediments based on the elemental concentrations of last depth of the offshore core (core 2)

Station	As	Cu	Pb	Zn	Mn
N1	108	5	32	92	32
N2	151	6	52	129	35
N3	60	3	44	83	16
N4	60	3	32	68	18
N5	361	11	82	262	63

ERICA Assessment Tool. The contribution of the internal and external dose rate to the total dose rate and the total dose rate of each radionuclide per organism is depicted in Fig. 5. In all cases, the total dose rates were more than two orders of magnitude lower than the screening levels for aquatic biota (400  $\mu\text{Gy h}^{-1}$ ) proposed by IAEA (1992) and UNSCEAR (1996). Phytoplankton received the maximum total dose rate (0.65  $\mu\text{Gy h}^{-1}$ ), where the main contributor was the internal dose rate portion. This is attributed to the radionuclides which are mainly alpha emitters ( $^{226}\text{Ra}$  and  $^{228}\text{Th}$ ). The Tool assumes secular equilibrium among radionuclides and their daughters, if the half-life of the latter is less than 10 days (Brown et al. 2008). This leads to the sum of the received doses of  $^{226}\text{Ra}$  and its six daughters and  $^{228}\text{Th}$  and its seven daughters, which are alpha emitters. The other organisms which reside near the seafloor (e.g., crustacean, polychaete worm), exhibited external dose rates, due to sediment activity concentrations. The upper and lower confidence levels of dose rate estimation are presented in Fig. 5 and were determined according to the estimated relative uncertainty of activity concentrations.

### Core sediment

#### Historical reconstruction

The profiles of natural radionuclides ( $^{226}\text{Ra}$ ,  $^{228}\text{Ac}$ ), trace metals (As, Cu, Pb, Zn), and major elements (Mn, Fe, Al) in the coastal core (core 1) indicated three periods of mining activities: (a) 1860–1900 (core’s lower part 38–52 cm), (b) 1900–1930 (core’s middle part 28–38 cm), and (c) 1930–1980 (core’s upper part 12–28 cm). Also the vertical distribution of the aforementioned parameters is also provided during 1980–2014, after the cessation of the mining industry (0–12 cm). The minimum values of metal and radionuclide concentrations were observed during 1860–1900 while the maximum ones during 1930–2014. In the period 1900–1930, some element concentrations increased linearly and remained constant (e.g.,  $^{226}\text{Ra}$ , As, Mn), while others exhibited a peak (e.g., Cu, Pb, Al) with maximum observed value around the year of 1920 (Fig. 3a, b, as well as Fig. S1a–S1h of the Supporting Information document).

The minimum values of radionuclides and metals obtained during 1860–1900 are indicative of the existing slag and/or waste impact in the region. These ancient slags and wastes were present in the whole region of Lavreotiki, due to mining activities which lasted from 3000 BC until 100 BC and were the raw material exploited by Serpieris Company in 1875. The main ore exploited in the area, during ancient times, was galena for the production of Ag and Pb. During 1875–1900, Serpieris Company started by exploiting the

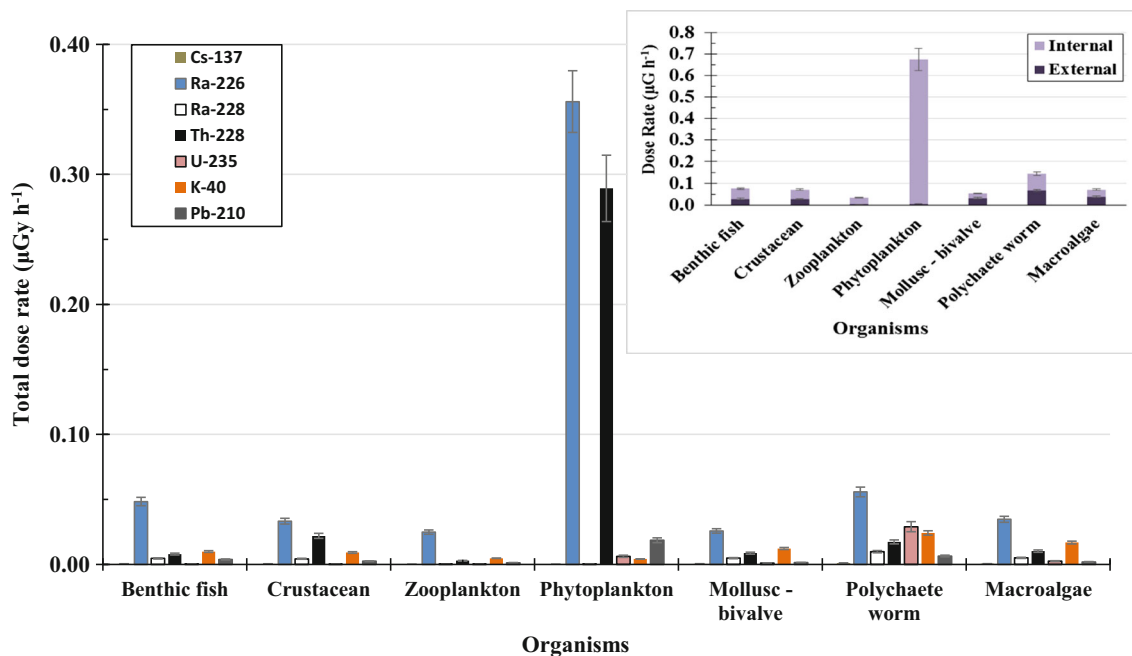


**Fig. 5** The internal, external, and total dose rate of marine organisms at Oxygono Bay. The upper and lower confidence levels of dose rate estimation were determined according to the estimated relative uncertainty of activity concentrations

ancient slags and continued by exploiting mixed sulfide ores (containing Zn), also for the production of Ag, Pb.

Around the year of 1920, an increment of radionuclide and metal concentration was observed in the core profile. During the period 1920–1930, the metal concentration of Pb and Cu decreases drastically while that of As, Zn, and Mn remains constant at the maximum obtained values. The increase of radionuclide and metal concentration from 1900 to 1920 is associated with the newly discovered floatation method which was immediately adopted in the exploitation activities. Although the floatation method exhibited higher efficiency in the metal recovery from the mineral, only Pb was exploited and As, Zn, and Mn were remained in the disposal material. The produced tailings were also characterized by finer grains compared to previous periods of operation, as revealed in the mud content profile (20–40%) (Fig. 3d).

However, in the year around 1920, the Pb concentration in the core sediment was elevated due to the exploitation of oxidized ores, despite the adaptation of the floatation method. Thus, in the following period during 1920–1930, the decrease of Pb concentration may be attributed to higher recovery rates of Pb from the mineral without using oxidized ores. The use of oxidized ores contributed also to the observed peaks at Cu and Al profiles, since these ores contained small quantities of Cu, as well as slimes of shale enriched in Al. Then, after the cessation of oxidized mineral use, the aforementioned metal concentrations were reduced at the levels of pre-operational periods (around 1875). The different type of incorporated exploiting methods could be also revealed by the peaks at Cu, Pb, and Al mass flux profiles during 1900–1930.

After 1980, all metals exhibited similar values with the previous period (1930–1980), despite of the cessation of mining in Lavrio area (early 1980s). This observation may be attributed to the strong north winds and currents that transport sediment from Thorikos to Oxygono Bay after resuspension and deposition processes. Other processes, like rain-wash may transfer material into the coast originated from the adjacent contaminated terrestrial part.

Nevertheless, the calculated mass fluxes in the coastal sediment core did not provide more information for the reconstruction of the aforementioned events, but can be used as baseline information of the temporal mass deposition at the study area.

### Enrichment factors

The enrichment factor (EF) profiles of As, Cu, Pb, Zn, and Mn, determined for the coastal sediment core (core 1), are depicted in Fig. 6. The calculated EFs using as background values those of the continental shale are depicted in Fig. 6a. According to Birch and Davies (2003), extremely severe enrichment in As, Pb, and Zn and moderately severe enrichment

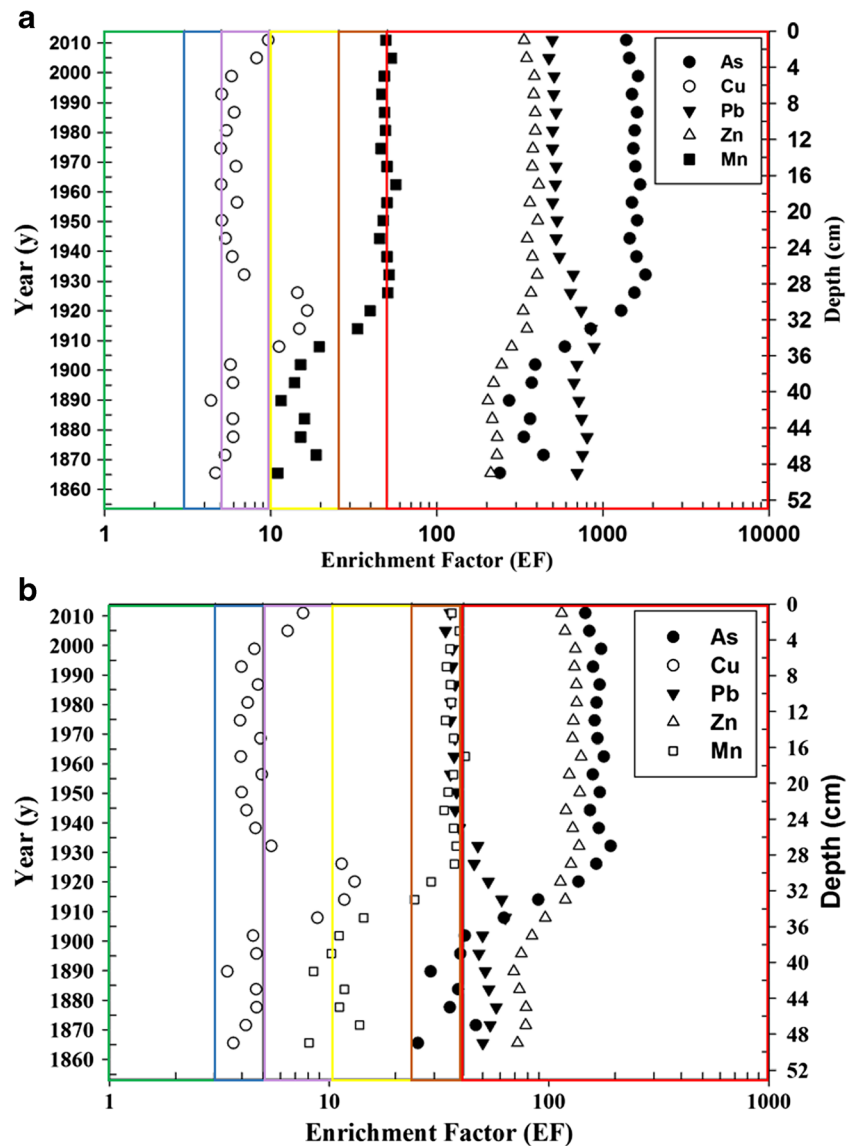
in Cu characterize the whole core. Very severe and severe enrichment in Mn characterizes the upper and the remaining (middle and lower) part of the core, respectively. The order of enrichment was  $As > Pb > Zn > Mn > Cu$ .

The EFs were estimated using another background level, the one of the last depth slice of the offshore core (core 2). In order to verify the selection of this background sample, the EF estimation using the concentrations of continental crust shale as reference values was achieved. Thus, the EF determination gave EF values of 1, 9, 1, 14, and 3 for Mn, As, Cu, Pb, and Zn, respectively. According to the adopted classification the background selection of Mn, Cu and Zn were accurate, since the determined EFs revealed no or minor enrichment. However, the last depth layer of the offshore core (core 2) was not suitable as reference sample, because it was characterized moderately severely and severely enriched in As and Pb, respectively. On the other hand, the metal concentrations of the last depth sample were found  $174 \mu\text{g g}^{-1}$ ,  $19 \mu\text{g g}^{-1}$ ,  $9 \mu\text{g g}^{-1}$ ,  $42 \mu\text{g g}^{-1}$ , and  $42 \mu\text{g g}^{-1}$  for Mn, As, Cu, Pb, and Zn, respectively and they were similar to or below the values of these elements in the shale of continental crust (Mn:  $850 \mu\text{g g}^{-1}$ , As:  $13 \mu\text{g g}^{-1}$ , Cu:  $45 \mu\text{g g}^{-1}$ , Pb:  $20 \mu\text{g g}^{-1}$ , Zn:  $95 \mu\text{g g}^{-1}$ ). The explanation of this paradox is the normalizer element (Al) concentrations in the offshore core of last depth slice ( $12 \cdot 10^3 \mu\text{g g}^{-1}$ ) and shale ( $80 \cdot 10^3 \mu\text{g g}^{-1}$ ). The study area is characterized by low Al concentrations, eight times lower than those of the shale, thus the adopted classification gave different signals, at first. The paradox of EF different signal and the low concentrations of the metals of interest supports the idea to perform EF calculations using as background/reference sites the neighboring area (deep layer of offshore core) and the global approach.

The calculated EFs using as background values those of the offshore core last depth layer are displayed in Fig. 6b and exhibited, up to an order of magnitude, lower values than those mentioned above. However, the enrichment classification did not change for As, Zn, and Mn, while altered generally, from extremely severe to very severe and from moderately to moderate severe enrichment in Pb and Cu, respectively. The order of enrichment also changed as follows:  $As > Zn > Pb > Mn > Cu$ . The maximum values of EF for As, Zn, and Mn were estimated during 1920–2014, indicating that the anthropogenic influence in the area occurred mainly during the last century. However, the distinct peaks at the EF profiles of Pb and Cu during 1900–1930 revealed this period as the most influenced due to the anthropogenic activities, where in the case of Cu the classification changed from moderate to severe enrichment. This short-term anthropogenic impact can be attributed to the different mining methods used in the ore exploitation during this period, as mentioned in “[Historical reconstruction](#)” section.



**Fig. 6** The depth profiles of enrichment factors (EFs) of As, Cu, Zn, Pb, and Mn of Oxygono Bay (core 1). **a** The depth profiles of enrichment factors (EFs) of As, Cu, Zn, Pb, and Mn. The element of Al and the elemental concentrations of the shale of the continental crust (Wedepohl 1995) were used for the estimation of EFs. The green color represents no or minor enrichment, the blue moderate enrichment, the purple moderately severe enrichment, the yellow severe enrichment, the orange very severe enrichment, and the red extremely severe enrichment. **b** The depth profiles of enrichment factors (EFs) of As, Cu, Zn, Pb, and Mn. The element of Al and the elemental concentrations of the offshore core (core 2) last depth were used for the estimation of EFs. The green color represents no or minor enrichment, the blue moderate enrichment, the purple moderately severe enrichment, the yellow severe enrichment, the orange very severe enrichment, and the red extremely severe enrichment



**Comparison of core sediment with neighboring areas and international values of reference**

Despite the higher concentrations measured in the upper part (0–28 cm) of the coastal sediment core, they were similar with those obtained in the surface sediment of the neighboring areas and they were well below the world median values for soil (UNSCEAR 2000) (see Table 4). Additionally, the concentrations of As, Cu, Pb, Zn, and Mn in the coastal core exhibited similar values with those of the surface sediment at Oxygono Bay (2014 and 2016 samplings) and they were well above the values measured in the offshore core, the neighboring areas (Zotiadis and Kelepertzis 1997; Michalopoulou et al. 2015), the shale of the continental crust (Wedepohl 1995), and the upper level of sediment quality guidelines (OMEE 1993; USEPA 2000; UNSCEAR 2000) (Fig. 7). This difference in the data sets provides a significant

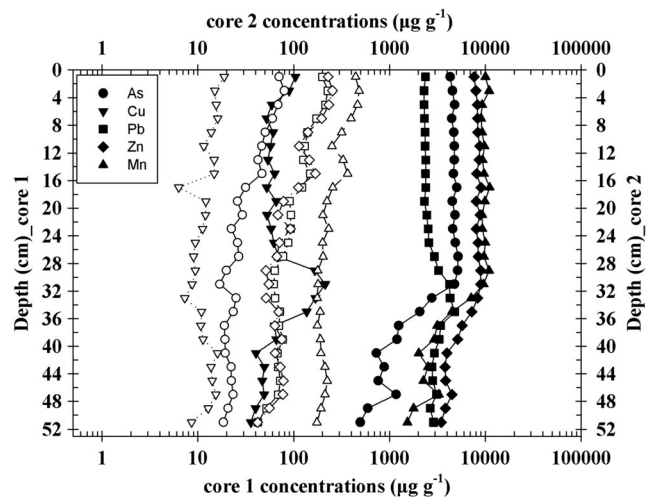


**Fig. 7** The concentrations of trace metals (As, Cu, Pb, Zn, and Mn) in the coastal (core 1) (black dots) and the offshore (core 2) (white dots) sediment cores

information about the temporal and spatial contamination degree produced by the past mining activities during the last years.

The minimum and maximum metal concentrations of the offshore core were similar to those of Perdica, Thorikos, and Delenia Bay, the low values obtained in Lavreotiki peninsula (Zotiadis and Kelepertzis 1997) and the concentrations of shale. However, the minimum values measured in the deep slice of the offshore core were similar to or below the low level of sediment quality guidelines. The slight difference among the results of the deep layer of the offshore core with the values of the shale and sediment quality guidelines strengthens the assumption for the selection of the deep layer of the core as background sample. The maximum values of metal concentration were obtained in the surface slices of the offshore core and were above or similar to the low level of sediment quality guidelines, indicating possible influence of the mining activities at 2 km away from the Lavrio coast, towards Makronisos Island. Thus, further investigation in the seafloor between Oxygono Bay (coastal core) and Makronisos Island (offshore core) is needed.

## Summary and conclusions

In the present study, the temporal and spatial investigation in Oxygono Bay was accomplished. The dating analysis using  $^{210}\text{Pb}$  was utilized for the reconstruction of the anthropogenic influence in the area due to mining and was verified by the history of the mining activities in the specific region. The assessment of this impact was also determined using enrichment factors and comparing with neighboring areas and sediment quality guidelines.

Oxygono Bay was greatly influenced—spatially and temporally—by the mining activities due to the dumped mine wastes in the terrestrial environment of the operation area. The identified operational periods were the following: (a) the period 1860–1900 where minimum values of all metals were observed due to the applied low efficiency of the recovery method and the use of ancient slags as raw material, (b) the period 1900–1930 where all metals and  $^{226}\text{Ra}$  concentrations were increased due to the improvement of the recovery method that was implemented in the mining process, and (c) the period 1930–1980 where the almost constant values of metal concentrations reveal the establishment of the applied mining method. The waste materials in the area are evident during the period of 1980–2014, although the mine operations stopped in the early 1980s. This evidence is demonstrated from the metal concentrations, the metal mass flux, and the EF values that remain similar compared to the previous operational mining period (1930–1980).

The different type of raw material and exploitation methods incorporated in the area were represented as distinctive peaks

at the Pb and Cu concentration and mass flux and EF profiles during 1900–1930. However, the mass fluxes obtained in the bay can be used only as baseline information. The order of enrichment in the area was  $\text{As} > \text{Zn} > \text{Pb} > \text{Mn} > \text{Cu}$  for both surface and core sediments at all periods.

The dose rate assessment for natural and  $^{137}\text{Cs}$  radioactivity was also incorporated by ERICA Tool and the obtained values were well below of those adopted by ERICA.

**Acknowledgments** Mrs F.K. Pappa would like to acknowledge A.G. Leventis Foundation for the financial support of her PhD thesis. The crew of the R/V AEGEAO and Dr. G. Rousakis are also acknowledged for providing the offshore sediment core between Lavreotiki peninsula and Makronisos Island.

## References

- Aberg G, Charalampides G, Fosse G, Hjelmeth H (2001) The use of Pb isotopes to differentiate between contemporary and ancient sources of pollution in Greece. *Atmos Environ* 35:4609–4615
- Abril JM, San Miguel EG, Rruiz-Canovas C, Casaa-Ruiz M, Bolivar JP (2018) From floodplain to aquatic sediments: radiogeochronological fingerprints in a sediment core from the mining impacted Sancho Reservoir (SW Spain). *Sci Total Environ* 631–632:866–878
- Ademola AK, Bello AK, Adejumbi AC (2014) Determination of natural radioactivity and hazard in soil samples in and around gold mining area in Itagunmodi, south-western, Nigeria. *J Radiat Res Appl Sci* 7: 249–255
- Alexakis D (2011) Diagnosis of stream sediment quality and assessment of toxic element contamination sources in East Attica, Greece. *Environ Earth Sci* 63:1369–1383
- Appleby PG, Oldfield F (1978) The calculation of lead-210 dates assuming a constant rate of supply of unsupported  $^{210}\text{Pb}$  to the sediment. *Catena* 5:1–8
- Arogunjo AM, Hollriegl V, Giussani A, Leopold K, Gerstmann U, Veronese I, Oeh U (2009) Uranium and thorium in soils, mineral sands, water and food samples in a tin mining area in Nigeria with elevated activity. *J Environ Radioact* 100(3):232–240
- Australian and New Zealand Environment and Conservation Council (ANZECC) (2000) Aquatic ecosystems—rationale and background information, National Water Quality Management Strategy, paper No 4, Vol. 2, chapter 8
- Balogun FA, Mokobia CE, Fasasi MK, Ogundare FO (2003) Natural radioactivity associated with bituminous coal mining in Nigeria. *Nucl Inst Methods Phys Res A* 505(1–2):444–448
- Batista MJ, Abreu MM, Pinto MS (2007) Biogeochemistry in Neves Corvo mining region, Iberian pyrite belt, Portugal. *J Geochem Explor* 92:159–176
- Bech J, Corrales I, Tume P, Barcelo J, Duran P, Roca N, Poschenrieder C (2012) Accumulation of antimony and other potentially toxic elements in plants around a former antimony mine located in the Ribes Valley (Eastern Pyrenees). *J Geochem Explor* 113:100–105
- Becker A, Klock W, Friese K, Schreck P, Treutle HC, Spettel B, Duff MC (2001) Lake Suber See as a natural sink for heavy metals from copper mining. *J Geochem Explor* 74:205–217
- Birch GF (2017) Determination of sediment metal background concentrations and enrichment in marine environments – a critical review. *Sci Total Environ* 580:813–831
- Birch GF and Davies K (2003) A scheme for assessing human impacts on coastal aquatic environments using sediments, In: Coastal GIS,

- Woodcoffe C.D. and Furness R.A., Eds., Wollongong University Papers in Center for Maritime Policy, 14, Australia
- Brown JE, Alfonso B, Avila R, Beresford NA, Copplestone D, Prohl G, Ulanovsky A (2008) The ERICA tool. *J Environ Radioact* 99:1371–1383
- Cochran JK, Hirschberg DJ, Wang J, Dere C (1998) Atmospheric deposition of metals to coastal waters (Long Island sound, New York USA): evidence from saltmarsh deposits. *Estuar Coast Shelf Sci* 46:503–522
- Demetriades A (2010) Medical geology in Hellas: the Lavrion environmental pollution study, In: Medical Geology, O. Selinus et al. (eds), International Year of Planet Earth, Springer Science + Business Media B. V, 355-390, DOI [https://doi.org/10.1007/978-90-481-3430-4\\_13](https://doi.org/10.1007/978-90-481-3430-4_13)
- Eleftheriou G (2014). Estimation and spatial-temporal dispersion of radionuclides in the aquatic environment (PhD thesis), National Technical University of Athens (in Greek)
- Folk RL (1974) Petrology of the sedimentary rocks. Hemphill Publishing Company, Austin, p 182
- Gaafar I, El-Shershaby A, Zeidan I, El-Ahll LS (2016) Natural radioactivity and radiation hazard assessment of phosphate mining, Quseir-Safaga area, central eastern desert, Egypt. *NRIAG J Astron Geophys* 5:160–172
- Garcia-Ordiales E, Cienfuegos P, Roqueni N, Covelli S, Flor-Blanco G, Fontolan G, Loredó J (2017) Historical accumulation of potentially toxic trace elements resulting from mining activities in estuarine salt marshes sediments of the Asturias coastline (northern Spain). *Environ Sci Pollut Res*. <https://doi.org/10.1007/s11356-017-0449-5> (in press)
- Gomez-Gonzales MA, Garcia-Guinea J, Laborda F, Garrido F (2015) Thallium occurrence and partitioning in soils and sediments affected by mining activities in Madrid province (Spain). *Sci Total Environ* 536:268–278
- Gribov A and Krivoruchko K (2012) New flexible non-parametric data transformation for trans-Gaussian kriging. *Geostatistics Oslo (2012) Quantitative Geology and Geostatistics, Vol. 17: Part 1*, (pp 51–65), Netherlands: Springer
- Haralambides L, Sakellariadou F (2008) A pollutant dispersion model for the Piraeus, Lavrio and Rafina ports and the Elefsis Gulf. *Fresenius Environ Bull* 17(10a):1607–1614
- Hassan NM, Mansour NA, Fayez-Hassan M, Sedqy E (2016) Assessment of natural radioactivity in fertilizers and phosphate ores in Egypt. *J Taibah Univ Sci* 10:296–306
- Heaton B, Lambly J (1995) TENORM in the oil, gas and mineral mining industry. *Appl Radiat Isot* 46(6–7):577–581
- Hilal MA, Attallah MF, Mohamed GY, Fayez-Hassan M (2014) Evaluation of radiation hazard potential of TENORM waste from oil and natural gas production. *J Environ Radioact* 136:121–126
- Huang YJ, Chen CF, Huang YC, Yue QJ, Zhong CM (2015) Natural radioactivity and radiological hazards assessment of bone-coal from a vanadium mine in central China. *Radiat Phys Chem* 107:82–88
- International Atomic Energy Agency (IAEA) (1987) Preparation of gamma-ray spectroscopy reference materials RGU-1, RGTh-1 and RGK-1 report-IAEA/RL/148, Vienna, Austria
- International Atomic Energy Agency (IAEA) (1992) Effects of ionising radiation on plants and animals at levels implied by current radiation protection standards. Technical Reports Series No. 332, Vienna
- International Atomic Energy Agency (IAEA) (2004) Sediment distribution coefficients and concentration factors for biota in the marine environment. IAEA Report 422, Vienna
- Kalfas CA, Axiotis M, Tsabaris C (2016) SPECTRW: a software package for nuclear and atomic spectroscopy. *Nucl Inst Methods Phys Res A* 830:265–274
- Karageorgis AP, Anagnostou CL, Kaberi H (2005) Geochemistry and mineralogy of the NW Aegean Sea surface sediments: implications for river runoff and anthropogenic impact. *Appl Geochem* 20:69–88
- Kerfoot WC, Harting SL, Jeong J, Robbins JA, Rossmann R (2004) Local, regional and global implications of elemental mercury in metal (copper, silver, gold and zinc) ores: insights from Lake Superior sediments. *J Great Lakes Res* 30(Supplement 1):162–184
- Komnitsas K, Xenidis A, Adam K (1995) Oxidation of pyrite and arsenopyrite in sulphidic spoils in Lavrion. *Miner Eng* 8(12):1443–1454
- Kontopoulos A, Komnitsas K, Xenidis A, Papassiopi N (1995) Environmental characterisation of the sulphidic tailings in Lavrion. *Miner Eng* 8(10):1209–1219
- Kusin FM, Abd Rahman MS, Madzin Z, Jusop S, Mohamat-Yusuff F, Ariffin M, Mohd Syakirin MDZ (2017) The occurrence and potential ecological risk assessment of bauxite mine-impacted water and sediments in Kuantan, Pahang, Malaysia. *Environ Sci Pollut Res* 24:1306–1321
- Larsen TS, Kristensen JA, Asmund G, Bjerregerd P (2001) Lead and zinc in sediments and biota from Maarmorilik, west Greenland: an assessment of the environmental impact of mining wastes on an Arctic fjord system. *Environ Pollut* 114:275–283
- Li Y, Wang Y, Gou X, Su Y, Wang G (2006) Risk assessment of heavy metals in soils and vegetables around non-ferrous metals mining and smelting sites, Baiyin, China. *J Environ Sci* 18(6):1124–1134
- Li Z, Ma Z, Jan van der Kuijp T, Yuan Z, Huang L (2014) A review of soil heavy metal pollution from mines in China: pollution and health risk assessment. *Sci Total Environ* 468-469:843–853
- Liu H, Pan Z (2012) NORM situation in non-uranium mining in China. *Ann ICRP* 41(3–4):343–351
- Michalik B (2008) NORM impacts on the environment: an approach to complete environmental risk assessment using the example of areas contaminated due to mining activity. *Appl Radiat Isot* 66:1661–1665
- Michalopoulou V, Tsabaris C, Patiris DL, Androulakaki EG, Eleftheriou G, Kokkoris M, Pappa FK, Vlastou R (2015) Measurement of radionuclides and heavy metals concentration in surface sediments from the coastal zone of Lavreotiki peninsula, Proceedings of the 24th Hellenic Nuclear Society Symposium, 22–23 May, Ioannina
- Navarro MC, Perez-Sirvent C, Martinez-Sanchez MJ, Vidal J, Tovar PJ, Bech J (2008) Abandoned mine sites as a source of contamination by heavy metals: a case study in a semi-arid zone. *J Geochem Explor* 96:183–193
- Noli F, Tsamos P (2017) Seasonal variations of natural radionuclides, minor and trace elements in lake sediments and water in a lignite mining area of North-Western Greece. *Environ Sci Pollut Res*. <https://doi.org/10.1007/s11356-017-9801-z> (published online)
- Odumo OB, Mustapha AO, Patel JP, Angeyo HK (2011) Radiological survey and assessment of associated activity concentration of the naturally occurring radioactive materials (NORM) in the Migori artisanal gold mining belt of southern Nyanza, Kenya. *Appl Radiat Isot* 69:912–916
- Ontario Ministry of Environment and Energy (OMEE) (1993) Guidelines for the protection and management of aquatic sediment quality in Ontario Ministry of Environment and Energy, ISBN0-7778-9248-7.
- Panagopoulos I, Karayannidis A, Adam K, Aravossis K (2009) Application of risk management techniques for the remediation of an old mining site in Greece. *Waste Manag* 29:1739–1746
- Pappa FK, Tsabaris C, Ioannidou A, Patiris DL, Kaberi H, Pashalidis I, Eleftheriou G, Androulakaki AG, Vlastou R (2016) Radioactivity and metal concentrations in marine sediments associated with mining activities in Ierissos Gulf, North Aegean Sea, Greece. *Appl Radiat Isot* 116:22–33
- Patiris DL, Tsabaris C, Anagnostou CL, Androulakaki EG, Pappa FK, Eleftheriou G, Sgouros G (2016) Activity concentration and spatial distribution of radionuclides in marine sediments close to the estuary of Shatt al-Arab/Arvand Rud River, the Gulf. *J Environ Radioact* 157:1–15
- Pires do Rio MA, Amaral ECS, Fernandes HM, Rochedo ERR (2002) Environmental radiological impact associated with non-uranium

- mining industries: a proposal for screening criteria. *J Environ Radioact* 59:1–17
- Rose CL, McKay A, Toole J (1994) The use of the  $^{234}\text{Th}/^{238}\text{U}$  disequilibrium in studying surf-zone sediment processes in the eastern Irish Sea. *Mar Environ Res* 37:393–416
- Rowan JS, Barnes SJA, Hetherington SL, Lambers B, Parsons F (1995) Geomorphology and pollution: the environmental impacts of lead mining, Leadhills, Scotland. *J Geochem Explor* 52:57–65
- Saari HK, Schmidt S, Coynel A, Huguet S, Schafe J, Blanc G (2007) Potential impact of former Zn ore extraction activities on dissolved uranium distribution in the Riou-Mort watershed (France). *Sci Total Environ* 382:304–310
- Sakellariadou F, Haralambides L (2004) Lead, zinc, copper and iron partitioning spatial distribution in Lavrio port sediments. 37th Congr. of Mediterranean Science Commission. *Rapp Comm Int Mer Medit* 37:239
- Salbu B, Burkitbaev M, Stromman G, Shishkov I, Kayukov P, Uralbekov B, Rosseland BO (2013) Environmental impact assessment of radionuclides and trace elements at the Kurday U mining site, Kazakhstan. *J Environ Radioact* 123:14–27
- Salomons W (1995) Environmental impact of metals derived from mining activities: processes, predictions, prevention. *J Geochem Explor* 52:5–23
- Salomons W, Forstner U (1984) *Metals in the hydrocycle*. Springer-Verlag, Berlin
- Sanchez-Cabeza JA, Ruiz-Fernandez AC (2012)  $^{210}\text{Pb}$  sediment radiochronology: an integrated formulation and classification of dating models. *Geochim Cosmochim Acta* 82:183–200
- Sethy NK, Jha VN, Sutar AK, Rath P, Sahoo SK, Ravi PM, Tripathi RM (2014) Assessment of naturally radioactive materials in the surface soil of uranium mining area of Jharkhand, India. *J Geochem Explor* 142:29–35
- Shukurov N, Kodirov O, Peitzsch M, Kersten M, Pen-Mouratov S, Steinberger Y (2014) Coupling geochemical, mineralogical and microbiological approaches to assess the health of contaminated soil around the Almalyk mining and smelter complex, Uzbekistan. *Sci Total Environ* 476–477:447–459
- Skipperud L, Stromman G, Yunusov M, Stegnar P, Stegnar P, Uralbekov B, Tiloboev H, Zjazjev G, Heier LS, Rosseland BO, Salbu B (2013) Environmental impact assessment of radionuclide and metal contamination at the former U sites Taboshar and Digmai, Tajikistan. *J Environ Radioact* 123:50–62
- Spencer KL, Cundy AB, Croudace IW (2003) Heavy metal distribution and early-diagenesis in salt marsh sediments from the Medway Estuary, Kent, UK. *Estuar Coast Shelf Sci* 57:43–54
- Stamatis G, Voudouris K, Karefilakis F (2001) Groundwater pollution by heavy metals in historical mining area of Lavrio, Attica, Greece. *Water Air Soil Pollut* 128:61–83
- Tomlinson DL, Wilson JG, Harris CR, Jeffrey DW (1980) Problems in the assessment of heavy-metal levels in estuaries and the formation of a pollution index. *Helgoländer Meeresun* 33:566–575
- Tsabaris C, Eleftheriou G, Kapsimalis V, Anagnostou C, Vlastou R, Durmishi C, Kedhi M, Kalfas CA (2007) Radioactivity levels of recent sediments in the Butrint Lagoon and the adjacent coast of Albania. *Appl Radiat Isot* 65:445–453
- Tsabaris C, Bagatelas C, Dakladas T, Papadopoulos CT, Vlastou R, Chronis GT (2008) An autonomous in situ detection system for radioactivity measurements in the marine environment. *Appl Radiat Isot* 66:1419–1426
- Tsabaris C, Kapsimalis V, Eleftheriou G, Laubenstein M, Kaberi H, Plastino W (2012) Determination of  $^{137}\text{Cs}$  activities in surface sediments and derived sediment accumulation rates in Thessaloniki Gulf, Greece. *Environ Earth Sci* 67:833–843
- United Nations Scientific Committee on the Effects of Atomic Radiation (UNSCEAR) (1996) *Effects of radiation on the environment*. United Nations Scientific Committee on the effects of atomic radiation, report to the general assembly, annex I. United Nations, New York
- United Nations Scientific Committee on the Effects of Atomic Radiation (UNSCEAR) (2000) *Sources and effects of ionizing radiation*, United Nations Scientific Committee on the effects of atomic radiation, Report to general assembly with scientific annexes, United Nations, New York
- United States Environmental Protection Agency (USEPA) (2000) *Prediction of sediment toxicity using consensus-based freshwater sediment quality guidelines*, EPA 905/R-00/007, June 2000
- Valette-Silver N (1993) The use of sediment core to reconstruct historical trends in contamination of estuarine and coastal sediments. *Estuaries* 16(3B):577–588
- Vidmar T, Kanisch G, Vidmar G (2011) Calculation of true coincidence summing corrections for extended sources with EFFTRAN. *Appl Radiat Isot* 69:908–911
- Villa M, Manjon G, Hurtado S, Garcia-Tenorio R (2011) Uranium pollution in an estuary affected by pyrite acid mine drainage and releases of naturally occurring radioactive materials. *Mar Pollut Bull* 62: 1521–1529
- Wedepohl KH (1995) The composition of the continental crust. *Geochim Cosmochim Acta* 59(7):1217–1232
- Xenidis A, Komnitsas K, Papassiopi N, Kontopoulos A (1997) *Environmental implications of the mining activities in Lavrion, Engineering Geology and the Environment*, Marinos, Koukis, Tsiambaos and Stoumaras (eds), Balkema, Rotterdam, ISBN9054108770
- Xenidis A, Papassiopi N, Komnitsas K (2003) Carbonate-rich mining tailings in Lavrion: risk assessment and proposed rehabilitation schemes. *Adv Environ Res* 7:479–494
- Yellishetty M, Ranjith PG, Kumar DL (2009) Metal concentrations and metal mobility in saturated mine wastes in mining areas of Goa, India. *Resour Conserv Recycl* 53:379–385
- Zotiadis V and Kelepertzis A (1997) *Pollution of bottom sediments from the Aegean region south-east of the Lavreotiki Peninsula, as an impact of the mining activity of Lavrion sulfide deposits*, Greece, Engineering Geology and the Environment, Marinos, Koukis, Tsiambaos & Stoumaras (eds), Balkema, Rotterdam, ISBN9054108770